Targeted Delivery of Liposomal Chemo-Immunotherapy for Cancer Treatment

Yusheng Liu¹, Joonsu Han¹, Yang Bo¹, Rimsha Bhatta¹, Hua Wang^{1,2,3,4,5,6,7*}

¹Department of Materials Science and Engineering, University of Illinois at Urbana-Champaign, Urbana, IL 61801, USA. ²Cancer Center at Illinois (CCIL), Urbana, IL 61801, USA. ³Department of Bioengineering, University of Illinois at Urbana-Champaign, Urbana, IL 61801, USA. ⁴Carle College of Medicine, University of Illinois at Urbana-Champaign, Urbana, IL 61801, USA. ⁵Beckman Institute for Advanced Science and Technology, University of Illinois at Urbana-Champaign, Urbana, IL 61801, USA. ⁶Materials Research Laboratory, University of Illinois at Urbana-Champaign, Urbana, IL 61801, USA. ⁷Institute for Genomic Biology, University of Illinois at Urbana-Champaign, Urbana, IL 61801, USA.

*correspondence should be addressed to huawang3@illinois.edu

ABSTRACT

Chemo-immunotherapy that utilizes the immunomodulatory effect of chemotherapeutics has shown great promise for treating poorly-immunogenic solid tumors. However, there remains significant room for improving the synergy between chemotherapy and immunotherapy, including the efficient, concurrent delivery of chemotherapeutics and immunomodulators into tumors. Here we report the use of metabolic glycan labeling to facilitate cancer-targeted delivery of liposomal chemo-immunotherapy. 4T1 triple negative breast cancer cells can be metabolically labeled with azido groups, for subsequent targeted conjugation of dibenzocycoloctyne (DBCO)-bearing liposomes loaded with doxorubicin and imiquimod (R837) adjuvant via efficient click chemistry. The encased doxorubicin can induce the immunogenic death of cancer cells and upregulate the expression of CD47 and calreticulin on the surface of cancer cells, while R837 can activate dendritic cells for enhanced processing and presentation of tumor antigens. Targeted delivery of liposomes encapsulating doxorubicin and R837 to 4T1 tumors, enabled by metabolic glycan labeling and click chemistry, showed the promise to reshape the immunosuppressive tumor microenvironment of solid tumors. This cancer-targetable liposomal chemo-immunotherapy could provide a new approach to improving conventional chemotherapy.

Keywords. Immunotherapy, chemo-immunotherapy, metabolic glycan labeling, liposome, click chemistry.

INTRODUCTION

The past decades has witnessed the significant progress in clinical treatment of cancers, especially with the success of cancer immunotherapy including checkpoint blockades, chimeric antigen receptor (CAR) T cell therapy, and cancer vaccines. 1-3 However, the limited patient response rate, poor efficacy against many solid tumors, and occasionally severe side effects still limit the utility of immunotherapy.³⁻⁵ Currently, the vast majority of cancer patients are still suffering from conventional chemotherapy and radiation therapy with limited efficacy and severe side effects. As some chemotherapeutic agents can induce the immunogenic death of cancer cells and thus activate the immune system to assist in tumor clearance, 6-8 strategies to integrate chemotherapy with immunomodulatory agents have also been extensively explored. For example, doxorubicin (Dox), a first-line chemotherapeutics for treating breast cancer and other cancers, can upregulate the immunogenic markers of tumor cells and facilitate the release of tumor antigens from dying tumor cells, which was utilized for the development of combination therapies with checkpoint blockades or adjuvants. 9-11 Despite recent progress, the optimization of the synergy between chemotherapeutics and immunomodulators, upon a better understanding immunomodulatory effect within the tumor microenvironment, is still needed. 12-14 Ideally, tumor antigens released from dying tumor cells as a result of chemotherapy can be fully exploited by antigen presenting cells (e.g., dendritic cells (DCs)) for subsequent priming of antigen-specific effector T cells, as a part of the mechanism to reshape the immunosuppressive tumor microenvironment towards favoring immune cell infiltration and tumor killing.

Concurrent delivery of chemotherapeutics that functions towards tumor cells and immunomodulatory agents that modulate either DCs or T cells to the tumorous tissues remains another challenge. Targeted delivery of these molecules to the tumorous tissues could minimize off-target side effects. However, the separate modulation of tumor cells and immune cells by chemotherapeutics and immunomodulators within the tumor microenvironment limits the choice of suitable tumor-targeting technologies. For strategies that target the tumor matrix, 22-25 drug delivery systems can release co-loaded chemotherapeutics and immunomodulators in the tumor matrix which then function on tumor and immune cells, respectively. For strategies that target tumor cells, 26-28 we envision the use of non-metabolizable immunomodulators would be necessitated for the optimal synergy with chemotherapeutics. The internalized immunomodulators

can then be released from the dying tumor cells for subsequent modulation of immune cells in the tumor microenvironment. For example, doxorubicin (Dox) can induce the apoptosis and immunogenic death of tumor cells, and eventually facilitate the release of cellular constituents from dying tumor cells. By co-delivering Dox and R837,²⁹⁻³¹ a non-metabolizable adjuvant for activating DCs (also known as Imiquimod), into tumor cells, R837 can be released into the tumor microenvironment upon the death of tumor cells, activate DCs and facilitate the processing and presentation of tumor antigens by DCs, and thus amplify antitumor T cell responses.

Here we report the use of metabolic glycan labeling and click chemistry to achieve targeted delivery of liposomes co-encapsulating chemotherapeutics and adjuvants to tumor cells and tumorous tissues. Unnatural sugars such as tetraacetyl-N-azidoacetylmannosamine (Ac₄ManNAz) can undergo the metabolic glycoengineering processes and become expressed on the cell membrane in the form of glycoproteins and glycolipids. 32-36 The cell-surface azido groups can then mediate targeted conjugation of dibenzocyclooctyne (DBCO)-bearing agents via efficient and bioorthogonal click chemistry. ³⁷⁻⁴¹ Metabolic glycan labeling coupled with click chemistry has been successfully utilized for cancer-targeted delivery of therapeutics, diagnostics, and nanoparticles. 42,43 Upon covalent conjugation, agents can be gradually internalized by cells via the endocytic pathway. In this study, we aim to target liposomes co-encapsulating Dox and R837, a non-metabolizable adjuvant for activating DCs, to tumor cells. After covalent conjugation and cellular internalization, Dox is expected to induce the apoptosis of cancer cells, while the nonmetabolizable R837 remains intact intracellularly and eventually becomes released by the dead cancer cells. We show that liposomes co-encapsulating Dox and R837 can induce the immunogenic death of cancer cells and activation of DCs, and with simple DBCO modification, can be efficiently conjugated to azido-labeled cancer cells. In vivo metabolic labeling of tumor cells with azido groups, followed by administration of DBCO-modified Dox/R837-loaded liposomes, also manage to reshape the tumor microenvironment by activating DCs, repolarizing tumor-associated macrophages, and improving the tumor infiltration of T cells.

RESULTS and DISCUSSIONS

We first studied whether tetraacetyl-*N*-azidoacetylmannosamine (Ac₄ManNAz) can metabolically label 4T1 breast cancer cells with azido groups. After treating with Ac₄ManNAz for 48 h, cells

were incubated with DBCO-Cy5 for the detection of cell-surface azido groups. Flow cytometry analysis showed much higher Cy5 fluorescence intensity of Ac₄ManNAz-treated 4T1 cells than untreated cells (**Fig. 1a-b, Fig. S1**), indicating the successful metabolic labeling of 4T1 cells with azido groups. Ac₄ManNAz-mediated metabolic labeling efficiency of 4T1 cells was concentration-dependent (**Fig. S2a**). Higher concentrations of Ac₄ManNAz (> 25 μM) could result in enhanced metabolic labeling efficiency, but also exhibited a noticeable cytotoxicity (**Fig. S2b**). For these reasons, 25 μM Ac₄ManNAz was used in all subsequent *in vitro* experiments. Confocal imaging confirmed the significantly higher Cy5 fluorescence intensity of Ac₄ManNAz-treated cells than control cells, and showed a good overlay between Cy5 signal and membrane stain (**Fig. 1c**). To validate whether azido groups were expressed in the form of glycoproteins, we also performed western blot analysis of 4T1 cell lysates and detected the azido-tagged glycoproteins using DyLightTM 650-Phosphine that can conjugate with azido groups. As a result, Ac₄ManNAz-treated 4T1 cells, unlike control cells, showed various protein bands under the Cy5 fluorescence channel (**Fig. 1d**), demonstrating the successful azido labeling of cell-surface glycoproteins.

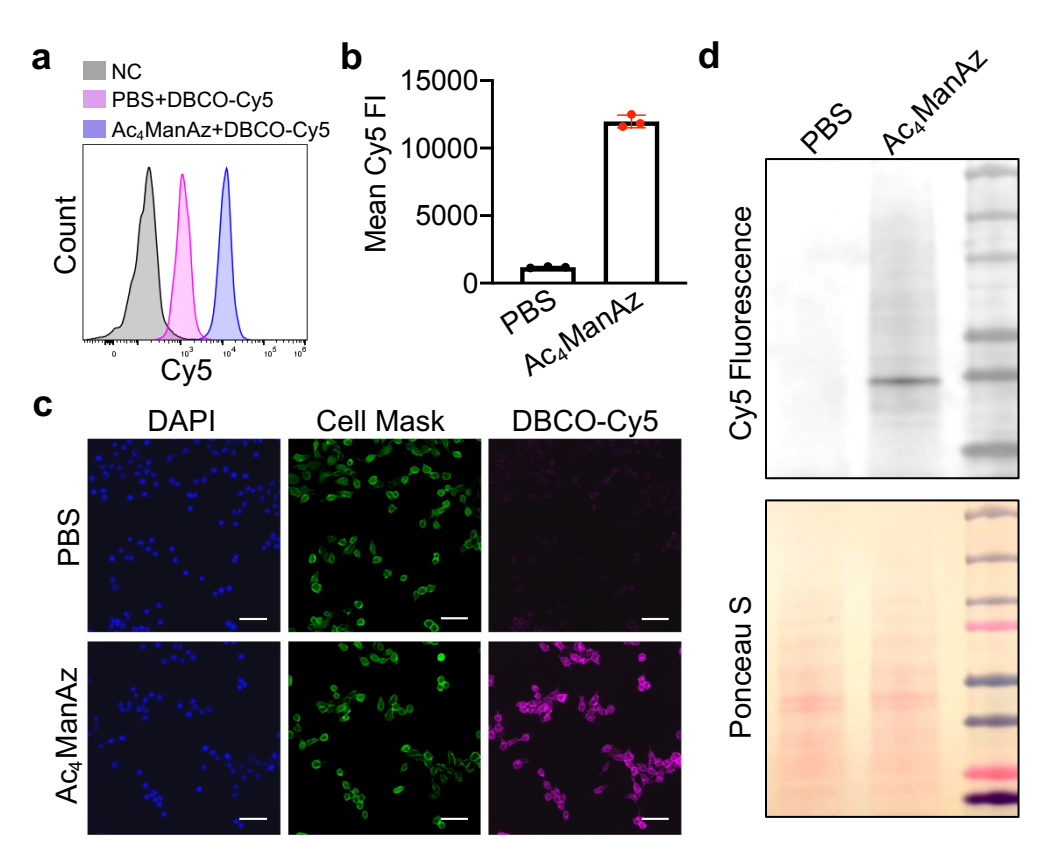


Fig. 1. Metabolic glycan labeling of 4T1 cancer cells with azido groups. 4T1 cells were incubated with Ac₄ManNAz (25 μ M) or PBS for 48 h, and then stained with DBCO-Cy5 for detection of cell-surface azido groups. (a) Representative Cy5 histograms of 4T1 cells for different

groups. 4T1 cells without any treatment were used as negative controls. (b) Mean Cy5 fluorescence intensity of 4T1 cells pretreated with Ac₄ManNAz (25 μM) and PBS, respectively. (c) Fluorescence images of Ac₄ManNAz- or PBS-pretreated 4T1 cells. Cell nuclei and membranes were stained with DAPI and Cell Mask, respectively. Scar bar: 50 μm. (d) Western blot analysis of azido-labeled glycoproteins. Azido-labeled proteins were conjugated with DyLightTM 650-Phosphine for fluorescence visualization. Ponceau S stains of whole protein bands were also shown.

We next synthesized DBCO-modified liposomes using DOPC, cholesterol, DSPE-PEG₂₀₀₀-DBCO at a molar ratio of 6: 4: 0.5, following the reported membrane extrusion method (Fig. 2a). Control liposomes without DBCO modification were synthesized similarly by replacing DSPE-PEG₂₀₀₀-DBCO with DSPE-PEG₂₀₀₀. The as-synthesized DBCO-liposomes have an average diameter of 133 nm and zeta potential of -11.3 mV (Fig. 2b, Fig. S3), similar to that of control liposomes (Fig. S4a). Dox and R837 can be easily encapsulated into the liposomes during the lipid film hydration step, with unloaded Dox and R837 removed via the size exclusion chromatography (Fig. S4b). The loaded Dox and R837 can be quantified via HPLC, and a loading of 25 µg/mg Dox and 12.5 μg/mg R837 can be easily achieved (Fig. S5a-b). To validate the successful incorporation of DBCO functionality, we extracted liposomal components with methanol and analyzed the extracts via HPLC. At a detection absorption wavelength of 254 nm where the non-aromatic structures would be invisible, the extracts of DBCO-modified, Dox/R837-loaded liposomes showed three main peaks (Fig. 2c). The first two peaks corresponded to Dox and R837, respectively, while the third peak at ~6.5 min corresponded to DBCO-lipid (Fig. 2c), which was further confirmed by the absorption spectrum (Fig. 2d). Prior to the in vitro cell targeting study, we also fabricated DBCOmodified, DID-loaded liposomes, using a similar encapsulation strategy to Dox and R837, to enable fluorescence tracking. 4T1 cells pretreated with Ac₄ManNAz or PBS for 48 h were incubated with DBCO-modified, DID-loaded liposomes for 30 min, and imaged under a confocal microscope. Compared to the control cells with azido-sugar treatment, 4T1 cells pretreated with Ac₄ManNAz showed a significantly higher DID fluorescence signal (Fig. 2e). Flow cytometry analysis also confirmed the higher DID signal in Ac₄ManNAz-pretreated 4T1 cells than control cells (Fig. 2f). The intracellular DID signal also increased with the concentration of DBCOmodified, DID-loaded liposomes (Fig. 2g). These experiments demonstrated that azido-labeled cancer cells can mediate targeted conjugation of DBCO-modified liposomes via efficient click chemistry.

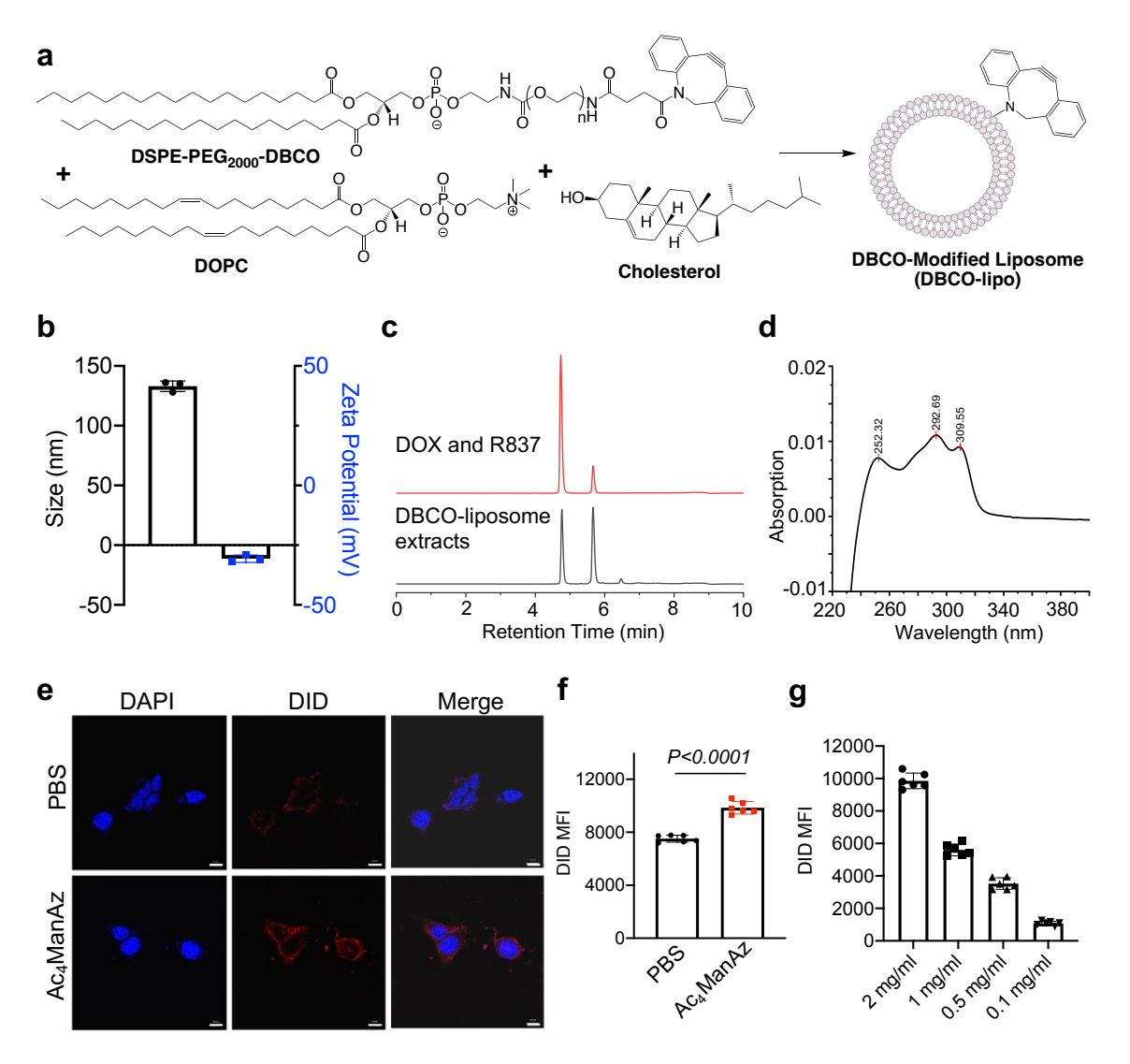


Fig. 2. Synthesis, characterization, and *in vitro* targeting effect of DBCO-modified liposomes. (a) Schematic illustration of synthesis of DBCO-modified liposomes from DSPE-PEG₂₀₀₀-DBCO, DOPC, and cholesterol. Unmodified liposomes were synthesized using DSPE-PEG₂₀₀₀. (b) Size and zeta potential of DBCO-lipo. (c) HPLC traces of a mixture of Dox and R837 or the extracts of Dox/R837-encapsulating DBCO-lipo. The detection wavelength was set at 254 nm. (d) UV absorption spectrum of DBCO-lipid as detected at ~6.5 min in (c). (e) Confocal images of 4T1 cells pretreated with Ac₄ManNAz or PBS for 48 h and then incubated with DID-encapsulating DBCO-lipo for 30 min. Scale bar: 10 μ m. (f) Mean Cy5 fluorescence intensity of 4T1 cells pretreated with Ac₄ManNAz or PBS for 48 h and then incubated with DID-encapsulating DBCO-lipo (2 mg/ml) for 30 min. (g) Mean Cy5 fluorescence intensity of 4T1 cells pretreated with Ac₄ManNAz and then incubated with different concentrations of DID-encapsulating DBCO-lipo for 30 min. All the numerical data are presented as mean \pm SD (0.01 < * $P \le 0.05$; ** $P \le 0.01$; *** $P \le 0.001$).

After demonstrating the *in vitro* targeting effect of DBCO-liposomes towards azido-labeled cancer cells, we next fabricated Dox/R837-loaded liposomes (lipoMix), Dox-loaded liposomes (lipoDox), and R837-loaded liposomes (lipoR837), respectively, and studied their ability to induce the immunogenic death of 4T1 breast cancer cells and B16F10 melanoma. Compared to control cells, 4T1 cells treated with Dox, lipoMix, or lipoDox for 16 h showed an upregulated expression of cell-surface calreticulin (Fig. 3a-b), which has been reported as a biomarker for the immunogenic death of cancer cells. 42-45 Compared to free Dox, lipoMix and lipoDox resulted in a comparable surface expression of calreticulin (Fig. 3a-b). In contrast, 4T1 cells treated with R837 or lipoR837 caused a negligible change in the surface expression of calreticulin (Fig. 3a-b), ruling out the effect of R837 on the immunogenic death of cancer cells. In addition to calreticulin, 4T1 cells treated with Dox, lipoMix, or lipoDox also upregulated the surface expression of the anti-phagocytic marker CD47 compared to control cells (Fig. 3c-d), which was previously demonstrated to aid in immunoevasion by cancer cells. R837 alone did not induce an increased expression of CD47 (Fig. 3c-d). 45-47 We also examined the surface expression of CD47 and calreticulin by 4T1 cells after treatment with Dox or LipoDox for 0, 2, 8, 16, 24, and 48 h, respectively. The expression levels of CD47 and calreticulin increased from 2 to 16 h and stayed stable after 16 h (Fig. S6a-b). It is noteworthy that 48-h incubation with Dox or LipoDox resulted in a significant reduction in 4T1 viability (Fig. S6c). A similar phenomenon was observed for B16F10 cells, i.e., an upregulated surface expression of calreticulin (Fig. 3e-f) and CD47 (Fig. 3g-h) by B16F10 cells treated with Dox, lipoMix, or lipoDox in comparison with control cells. These experiments demonstrated that Dox and Dox-loaded liposomes can induce the immunogenic death of cancer cells. We also studied whether in vitro targeting of lipoDox to cancer cells can improve the immunogenic cancer cell death. 4T1 cells were pretreated with Ac₄ManNAz to express azido groups on the cell surface, and then incubated with DBCO-lipoDox or lipoDox for 16 h. At all tested concentrations (50 nM, 500 nM, or 5 µM in Dox equivalents), DBCO-lipoDox induced a significantly higher expression of calreticulin on 4T1 cancer cells in comparison with lipoDox (Fig. 4a-c).

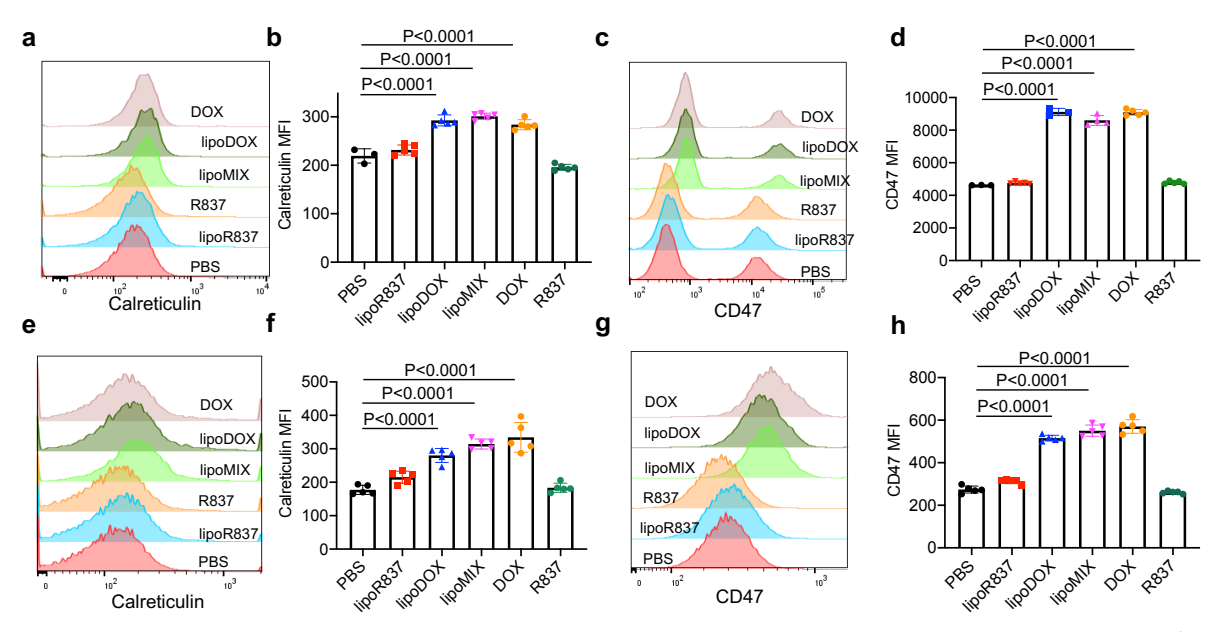


Figure 3. Dox-loaded liposomes can induce the immunogenic death of cancer cells. 4T1 breast cancer cells (a-d) or B16F10 melanoma (e-h) were incubated with free Dox, Dox-loaded liposomes (lipoDox), Dox/R837-loaded liposomes (lipoMix), R837-loaded liposomes (lipoR837), free R837, or PBS for 16 h, followed by staining with anti-CD47 and anti-calreticulin prior to flow cytometry analysis. The concentration of Dox and R837 was set at 500 nM and 330 nM, respectively. (a) Representative calreticulin histograms and (b) mean calreticulin fluorescence intensity of 4T1 cells after different treatments. Also shown are (c) representative CD47 histograms and (d) mean CD47 fluorescence intensity of 4T1 cells after different treatments. (e) Representative calreticulin histograms and (f) mean calreticulin fluorescence intensity of B16F10 cells after different treatments. Also shown are (g) representative CD47 histograms and (h) mean CD47 fluorescence intensity of B16F10 cells after different treatments. All the numerical data are presented as mean \pm SD (0.01 < * $P \le 0.05$; ** $P \le 0.01$; *** $P \le 0.001$).

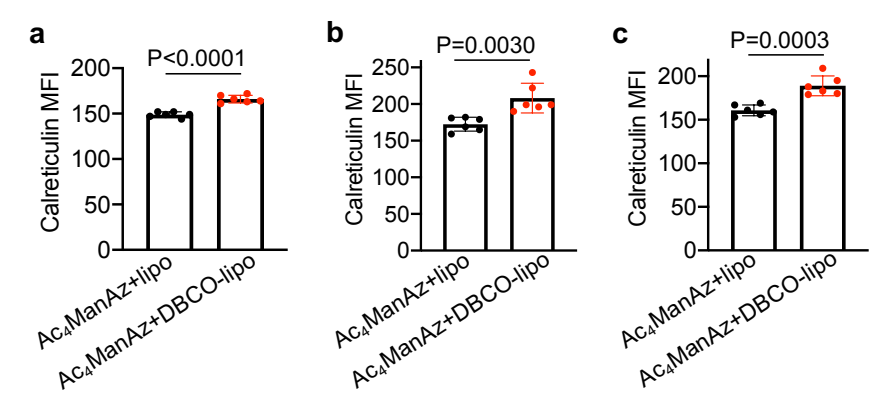


Figure 4. In vitro targeting of DBCO-liposomes to azido-labeled 4T1 cancer cells improves immunogenic cell death. 4T1 cells were pretreated with Ac₄ManNAz for 48 h, followed by incubation with DBCO-modified or unmodified, Dox-loaded liposomes at different Dox concentrations for 16 h. Shown are mean calreticulin fluorescence intensity of 4T1 cells after treatment with liposomes at a Dox concentration of (a) 50 nM, (b) 500 nM, or (c) 5 μ M. All the numerical data are presented as mean \pm SD $(0.01 < *P \le 0.05; **P \le 0.01; ***P \le 0.001)$.

After demonstrating the capability of Dox-loaded liposomes to induce the immunogenic death of cancer cells, we next studied whether R837-loaded liposomes can mediate the activation of DCs. Bone marrow-derived DCs (BMDCs) were incubated with free R837, R837-loaded liposomes (lipoR837), or PBS for 16 h, followed by FACS analysis of CD86 and MHCII expression levels (Fig. 5a). LipoR837 resulted in significantly improved activation of DCs in comparison with free R837, as evidenced by a higher percentage of CD86⁺MHCII⁺ DCs (**Fig. 5b**), a higher expression level of CD86 (Fig. 5c), and a higher expression level of MHCII (Fig. 5d). These experiments demonstrated that lipoR837 outperforms free R837 in activating DCs, presumably as a result of the enhanced accumulation of lipoR837 in endosomes where TLRs 7/8 (receptors for R837) exist. To better understand the crosstalk of cancer cells and DCs, we also studied whether Dox-treated cancer cells can improve the activation of DCs. 4T1 cells were treated with lipoDox, free Dox, or PBS for 24 h, followed by the removal of drug-containing cell media and addition of BMDCs. After 16-h incubation, the levels of cell-surface CD86 and MHCII on BMDCs were analyzed via flow cytometry (Fig. 6a). Compared to 4T1 cells pretreated with free Dox, cells pretreated with lipoDox resulted in a significantly higher expression level of CD86 and MHCII on DCs during the co-culture (Fig. 6b-d), demonstrating the superior ability of lipoDox to induce the apoptosis and immunogenic death of cancer cells for subsequent activation of DCs.

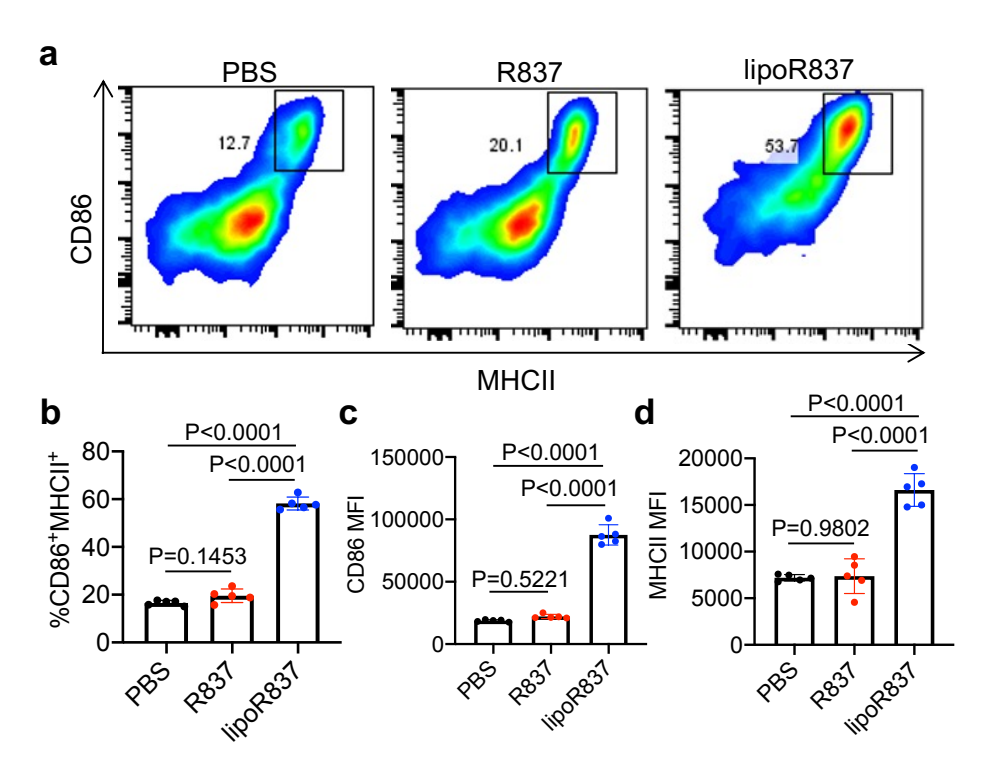


Figure 5. R837-loaded liposome outperforms R837 in improving the activation of DCs. BMDCs were incubated with free R837, R837-loaded liposomes (lipoR837), or PBS for 16 h, followed by FACS analysis of cell-surface CD86 and MHCII levels. (a) Representative CD86-MHCII plots of DCs after 16-h treatment with R837, lipoR837, or PBS. (b) Percentages of CD86+MHCII+ DCs following different treatments. Also shown are the mean (c) CD86 and (d) MHCII fluorescence intensity of DCs after different treatments. All the numerical data are presented as mean \pm SD (0.01 < * $P \le 0.05$; ** $P \le 0.01$; *** $P \le 0.001$).

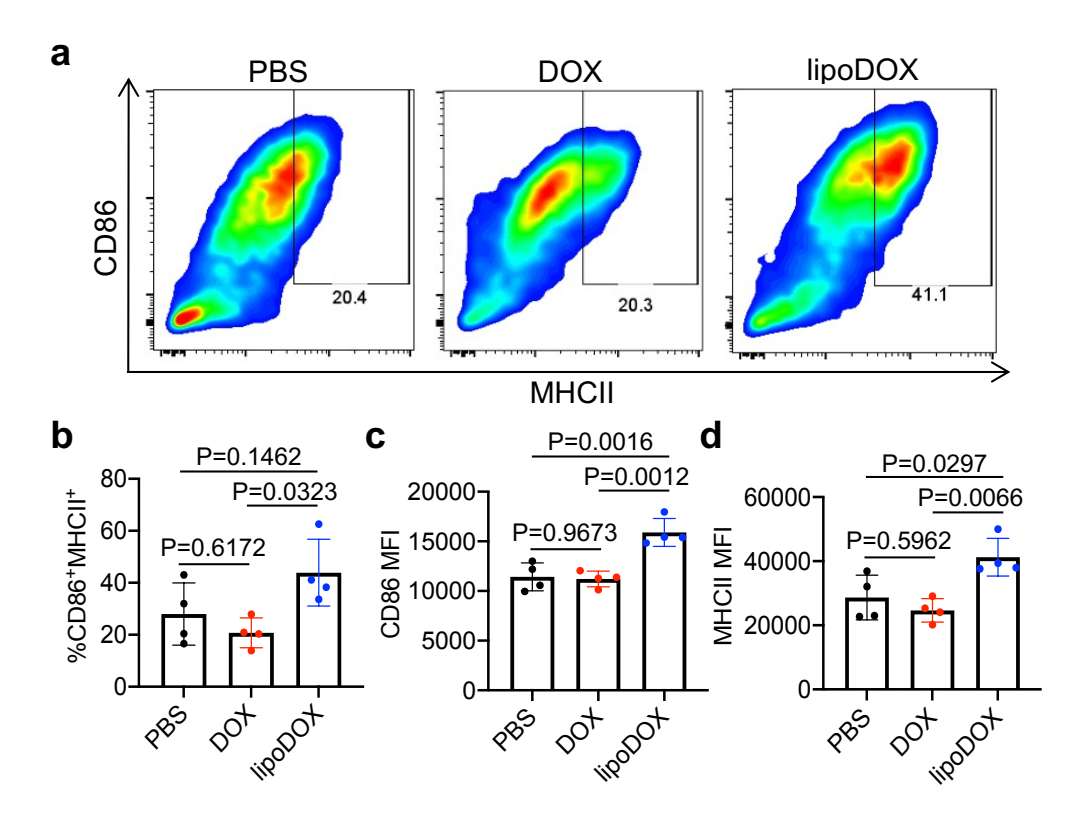


Figure 6. 4T1 cancer cells treated with Dox-loaded liposomes can induce the activation of DCs. 4T1 cells were treated with free Dox, Dox-loaded liposomes (lipoDox), or PBS for 16 h, and then co-culture with BMDCs for another 16 h. (a) Representative CD86-MHCII plots of DCs after 16-h co-culture with 4T1 cells. (b) Percentages of CD86+MHCII+ DCs following different treatments. Also shown are the mean (c) CD86 and (d) MHCII fluorescence intensity of DCs after different treatments. All the numerical data are presented as mean \pm SD (0.01 < * $P \le 0.05$; ** $P \le 0.01$; *** $P \le 0.001$).

After demonstrating the ability of Dox/R837-loaded liposomes to induce the immunogenic death of cancer cells and activation of DCs *in vitro*, we next studied whether targeting of Dox/R837-loaded liposomes to 4T1 tumors has the potential to reshape the immunosuppressive tumor microenvironment. Balb/c mice bearing established 4T1 tumors were intratumorally injected with Ac₄ManNAz or PBS, followed by injection of DBCO-modified, Dox/R837-loaded liposomes or a

mixture of Dox/R837 48 h later. After three days, tumors were harvested for immune analysis (**Fig. 7a**). Compared to the untreated group, azido-labeling coupled with DBCO-liposome was able to increase the population of CD11b⁺CD11c⁺ DCs in 4T1 tumors (**Fig. 7b**). Among the CD11b⁺CD11c⁺ DCs, a higher fraction of CD86⁺ population was also observed in tumors labeled with azido groups and then treated with DBCO-liposomes, in comparison with untreated mice (**Fig. 7c**). The targeting group also managed to increase the fraction of CD86⁺ M1-phenotype macrophages (**Fig. 7d**), decrease the fraction of CD206⁺ M2-phenotype macrophages (**Fig. 7e**), and increase the fraction of CD3⁺ T cells (**Fig. 7f**) in tumors compared to the untreated group. Compared to mice pretreated with PBS and then DBCO-liposomes, the targeting group resulted in a slight increase in the fractions of DCs, CD86⁺ DCs, and CD3⁺ T cells, and a slight decrease in CD206⁺ M2-phenotype macrophages (**Fig. 7b-f**), which we expect to further improve upon the optimization of the dose and dosing frequency of azido-sugars and DBCO-liposomes.

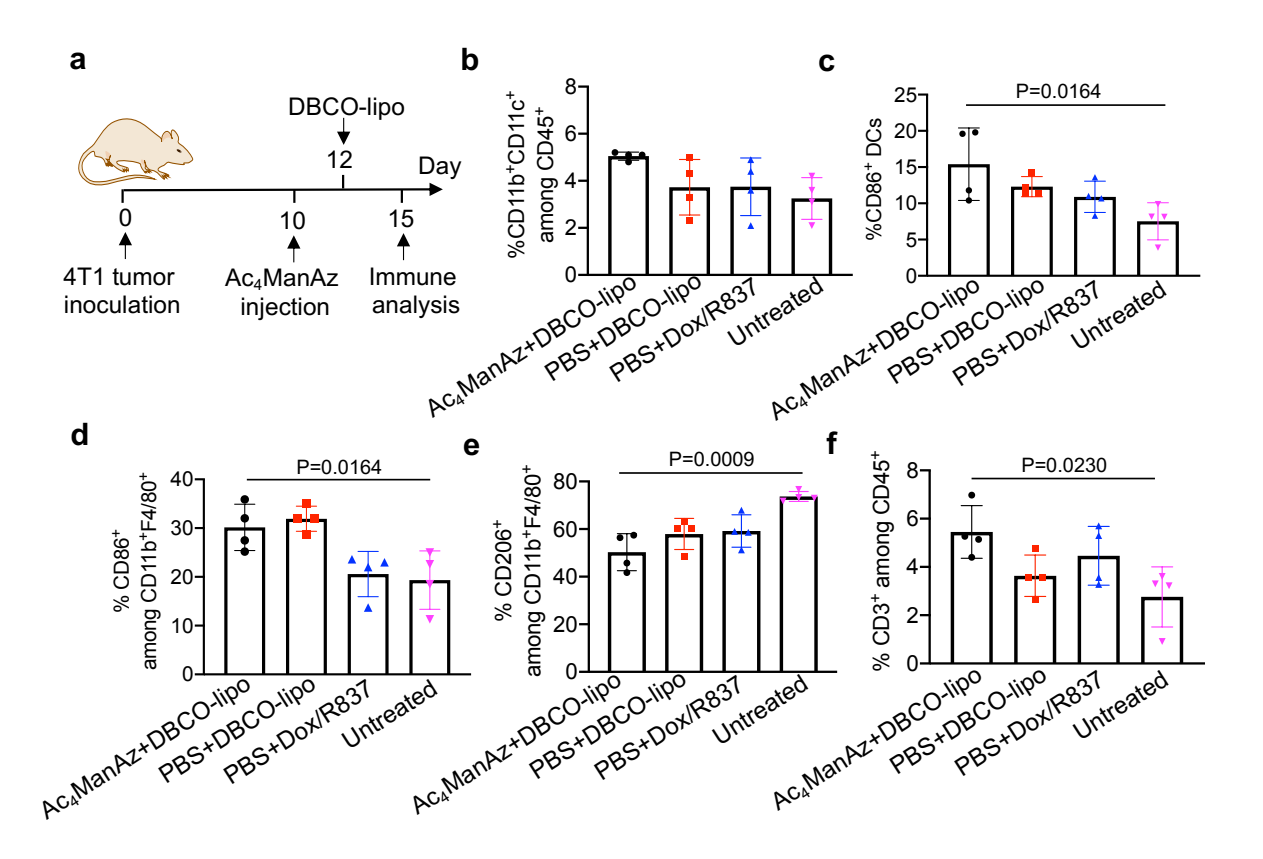


Figure 7. Azido-sugar coupled with Dox/R837-loaded DBCO-liposomes alters the immunosuppressive tumor microenvironment. (a-f) 4T1 tumors were inoculated on day 0, followed by intratumoral injection of Ac₄ManNAz (or PBS) on day 10 and DBCO-liposomes (or a mixture of Dox and R837) on day 12. On day 15, tumors were collected for immune analysis. (a)

Timeframe of tumor study. Shown are the percentages of (b) CD11b⁺CD11c⁺ DCs among CD45⁺ immune cells, (c) CD86⁺ cells among CD11b⁺CD11c⁺ DCs, (d) CD86⁺ cells among CD11b⁺F4/80⁺ macrophages, (e) CD206⁺ cells among CD11b⁺F4/80⁺ macrophages, and (f) CD3⁺ T cells among CD45⁺ immune cells in tumors after different treatment. All the numerical data are presented as mean \pm SD (0.01 < * $P \le 0.05$; ** $P \le 0.01$; *** $P \le 0.001$).

CONCLUSION

To summarize, we report the use of metabolic glycan labeling and click chemistry for targeted delivery of liposomal chemoimmunotherapy to cancer cells. Azido-sugars (e.g., Ac₄ManNAz) can metabolically label cancer cells with azido groups, for subsequent targeted conjugation of DBCO-bearing agents, including DBCO-modified liposomes, via efficient click chemistry. We show that liposomes co-encapsulating Dox and R837 were able to induce the immunogenic death of 4T1 and B16F10 cancer cells and the activation of DCs. Ac₄ManNAz-mediated metabolic labeling, coupled with DBCO-modified Dox/R837-loaded liposomes, was able to improve the immunogenic cancer death and activation of DCs *in vitro*, and showed the promise to reshape the immunosuppressive tumor microenvironment *in vivo*. Further optimization of the dose and dosing frequency of azido-sugars and DBCO-liposomes will enable the improved synergy between Dox and R837. Our strategy of targeting liposomal chemo-immunotherapy to tumors could provide an effective approach to improving conventional chemotherapy.

Materials and Methods

D-Mannosamine hydrochloride and other chemicals were purchased from Sigma-Aldrich (St. Louis, MO, USA) unless otherwise noted. DBCO-Cy5 was purchased from Thermo Fisher Scientific (Waltham, MA, USA). GM-CSF was purchased from PeproTech (Cranbury, NJ, USA). Primary antibodies used in this study, including PE-conjugated anti-CD11b (Invitrogen), PE/Cy7-conjugated anti-CD11c (Invitrogen), APC-conjugated anti-CD86 (Invitrogen), PE/Cy5.5-conjugated anti-CD3-ε (Invitrogen), Alexa Fluor 700-conjugated anti-CD8-α (Invitrogen), PE/Cy7-conjugated anti-PD-1 (Invitrogen), PE-conjugated anti-CTLA-4 (Invitrogen), APC-conjugated anti-LAG-3 (Invitrogen), and Alexa Fluor 700-conjugated anti-MHCII (Invitrogen) were purchased from Thermo Fisher Scientific (Waltham, MA, USA). Fixable viability dye efluor780 was obtained from Thermo Fisher Scientific (Waltham, MA, USA). All antibodies were diluted according to the manufacturer's recommendations. Small molecule compounds were run

on the Agilent 1290/6140 ultra-high performance liquid chromatography/mass spectrometer or the Shimadzu high performance liquid chromatography. Proton and carbon nuclear magnetic resonance spectra were collected on the Varian U500 or VXR500 (500 MHz) spectrometer. Fluorescent images were taken with a EVOS microscope (Thermofisher, Waltham, MA, USA). Fluorescence measurement was conducted on a Biotek plate reader (BioTek Instruments, Winooski, VT, USA). FACS analyses were collected on Attune NxT flow cytometers and analyzed on FlowjoTM 10. Statistical testing was performed using GraphPad Prism v8.

Cell lines and animals. The 4T1 cell line was purchased from American Type Culture Collection (Manassas, VA, USA). Cells were cultured in RPMI 1640 containing 10% FBS, and 100 units/mL Penicillin/streptomycin at 37°C in 5% CO2 humidified air. Female Balb/c mice were purchased from the Jackson Laboratory (Bar Harbor, ME, USA). Feed and water were available ad libitum. Artificial light was provided in a 12 h/12 h cycle. All procedures involving animals were done in compliance with National Institutes of Health and Institutional guidelines with approval from the Institutional Animal Care and Use Committee at the University of Illinois at Urbana-Champaign.

METHODS

Synthesis of Ac₄ManNAz. Mannosamine hydrochloride (2.3 mmol, 1.0 e.q.) was suspended in methanol, followed by the addition of sodium methoxide in methanol (25%, w/w) (2.3 mmol, 1.0 e.q.). The mixture was stirred until the mannosamine hydrochloride was dissolved. Triethylamine (1.1 e.q.) was then added to the solution upon vigorous stirring, following by the addition of chloroacetic anhydride (1.1 e.q.). The reaction mixture was stirred for overnight. Sodium azide (4.0 e.q.) was then added, and the reaction mixture was stirred at 65°C for another 12 h. Upon removal of the solvent under reduced pressure, pyridine was added to dissolve the residue. Acetic anhydride and a catalytic amount of DMAP were then slowly added to the mixture on a 0°C bath, with the mixture stirred for overnight. Water was added to quench the reaction and the solvent was removed on a rotavapor. The crude product was purified via silica gel column chromatography using ethyl acetate as the eluent (60% overall yield). ¹H NMR (CDCl₃, 500 MHz): δ (ppm) 6.66&6.60 (d, J= 9.0 Hz, 1H, C(O)NJCH), 6.04&6.04 (d, 1H, J=1.9 Hz, NHCHCJCH), 5.32-5.35&5.04-5.07 (dd, J=10.2, 4.2 Hz, 1H, CHJCHCHCJCHCHCH), 5.22&5.16 (t, J=9.9 Hz, 1H, CHJCHCHCJCHCHCJH), 4.60-4.63&4.71-4.74 (m, 1H, NHCJCHCHO), 4.10-4.27 (m, 2H, CJCHCHCHCJH),

4.07 (m, 2H, C(O)C H_2 N₃), 3.80-4.04 (m, 1H, CH₂CHCHCH), 2.00-2.18 (s, 12H, C H_3 C(O)). ¹³C NMR (CDCl₃, 500 MHz): δ (ppm) 170.7, 170.4, 170.3, 169.8, 168.6, 168.3, 167.5, 166.9, 91.5, 90.5, 73.6, 71.7, 70.5, 69.1, 65.3, 65.1, 62.0, 61.9, 52.8, 52.6, 49.9, 49.5, 21.1, 21.0, 21.0, 20.9, 20.9, 20.9, 20.8. ESI MS (m/z): calculated for C₁₆H₂₂N₄O₁₀Na [M+Na]⁺ 453.1, found 453.1.

Synthesis of DBCO-liposomes. Different lipids dissolved in the chloroform (10 mg/ml) were added to the glass vial with a composition of DOPC: CHOL: DSPE-PEG₂₀₀₀-DBCO = 6: 4: 0.5 (molar ratio). DSPE-PEG₂₀₀₀-DBCO was replaced with DSPE-mPEG₂₀₀₀ to synthesize the control liposome. The solvent was removed on a rotary evaporator to form a thin lipid film on the vial wall. The vial was further freeze-dried overnight to completely remove the solvent. PBS was added to the vial to yield a 10 mg/mL lipid solution, which was vortexed for 30 min at room temperature to hydrate the lipid film. After water bath sonication for 15 min, the resulting liposomes were further purified via a membrane extrusion method by passing through a 100 nm membrane 8 times with the Avanti extruder.

Loading of R837 and DOX into liposomes. DOX and R837 were encapsulated into the liposomes during the hydration process. Briefly, an equal volume of DOX (2 mg/ml in H₂O) and R837 (2 mg/ml in pH=2 HCl a.q. solution) were mixed to yield a mixture of 1 mg/ml DOX and 1 mg/ml R837. The mixture was added to dry lipid film, followed by 30-min vortex at room temperature to hydrate the lipid film. The lipid solution was then sonicated on a water bath for 15 min and extruded through a 100 nm membrane 8 times to yield liposomes. To remove the unencapsulated DOX and R837, liposomes were further purified by passing through a size exclusion column with PBS as the eluent. The encapsulated DOX and R837 was quantified with HPLC. The size and zeta potential of liposomes were characterized on a Malvern dynamic light scattering (DLS).

Synthesis of DID labeled DBCO-liposome. DID was encapsulated into the liposomes during the lipid film formation step. DID in methanol was added to the lipid mixture, followed by the removal of solvents on a rotary evaporator to form a lipid film. The lipid film was further freeze-dried overnight, and hydrated with PBS. The lipid solution was then sonicated on a water bath for 15 min and extruded through a 100 nm membrane 8 times to yield liposomes.

In vitro metabolic glycan labeling and flow cytometry detection. 4T1 cancer cells were seeded in a 6-well plate with a density of 2×10⁵ cells per well, and Ac₄ManNAz was added with a final concentration of 25 μM. A 50 mM stock solution of Ac₄ManNAz in DMSO was diluted with PBS to yield different concentrations. After incubated for 48 h, cells were washed with PBS for three times, followed by the incubation with 50 μM DBCO-Cy5 in Opti-MEM for 30 min. Cells were then detached from the plate with trypsin, washed with FACS buffer twice, and resuspended in FACS buffer containing 1% paraformaldehyde, prior to flow cytometry analysis.

Fluorescence imaging of metabolically labeled cells. 2×10^4 4T1 cells in 1 mL of DMEM were seeded into a 6-well plate with glass coverslips, and Ac₄ManNAz was added with a final concentration of 25 μ M. After incubated for 48 h, cells were washed with PBS for three times, followed by the incubation with 50 μ M DBCO-Cy5 in Opti-MEM for 30 min. After washing, cells were stained with the Membrane Green and DAPI following the manuals, fixed with 4% paraformaldehyde, and imaged under a fluorescence microscope.

Western blot analysis of azido-labeled cells. 2×10⁵ 4T1 cells in 5 mL of medium was seeded in to a culture dish in the presence or absence of 25 μM AAM, and cultured for 48 h. After washing with PBS, cells were lifted with trypsin and harvested. To each cell pellet, ice-cold cell lysis buffer (1% SDS, 100 mM Tris·HCl, pH 7.4) with 1x protein inhibitor cocktail was added, and the sample was sonicated for 5 min on an ice bath. Sonicated cell lysates were placed at 4°C for 30 min to further dissolve the proteins. The cell debris was removed by centrifugation with 21,000 g at 4°C for 10 min. The protein concentration in the supernatant was determined by bicinchoninic acid (BCA) protein assay (Pierce, IL, USA) and was adjusted to 2 mg/mL. To 10 μL of the solution, 0.5 μL DyLightTM 650-Phosphine (2 mM in DMSO) was added. The mixture was placed in 37°C for overnight. 2x SDS-PAGE loading buffer was then added, and 10 μL of each sample was loaded to 4-12% SDS-PAGE gels after heating at 95°C for 5 min. After SDS-PAGE gel electrophoresis, protein bands were transferred to the nitrocellulose membrane. The membrane was imaged on a Quan800 under the Cy5 channel. Protein bands were also confirmed by the Ponceau S staining.

Flow cytometry analysis of DBCO-liposome conjugation to azido-labeled 4T1 cells. 2x10⁴ 4T1 cells are seeded to a 6-well plate, followed by the addition of Ac₄ManNAz with a final

concentration of 25 μ M. After incubation for 48 h, cells were washed with HBSS, and incubated with different concentrations (2, 1, or 0.5 mg/mL) of DID-loaded DBCO-liposomes for 30 min at 37°C. After washing with PBS for three times, cells were treated with 0.25% trypsin and harvested for flow cytometry analysis.

Immunogenic death of 4T1 and B16F10 cells in vitro. 4T1 or B16F10 cells were seeded in a 96-well plate with a density of 2x10⁴ cells per well, and allowed to attach for overnight. Cells were then incubated with free Dox, free R837, Dox-loaded liposomes, R837-loaded liposomes, Dox/R837-loaded liposomes, or PBS for 16 h. The concentrations of Dox were set at 50, 500, or 5000 nM. The concentrations of R837 were set at 33, 330, or 3300 nM. The supernatant was removed and cells were lifted by treating with 0.25% trypsin. After washing with cold FACS buffer twice, cells were incubated with anti-CD47-FITC and Rabbit anti-Calreticulin primary antibody at 4°C for 30 min. After washing, Goat-anti-Rabbit-Cy5 secondary antibody and Fixable Viability Dye eFluor™ 780 was added to stain cells at 4°C for 30 min. Cells were then fixed with 0.4% PFA solution and analyzed on a flow cytometer.

In vitro BMDC activation. BMDCs were isolated from the tibia and femur of C57BL/6 mice following the previously reported method. Cells on day 6 or 7 were used. BMDCs were seeded to a 96-well plate with a density of 4×10⁴ cells per well, and different forms (free or liposome) and concentration (high, medium or low) of Dox and R837 were added. After 16 h, cells were stained with APC-conjugated anti-CD11c, PE-conjugated anti-CD86, Alexa Fluor 700-conjugated anti-MHCII, and Fixable Viability Dye eFluor™ 780 for 30 min at 4°C. Cells were then washed, fixed with 0.4% PFA, and resuspended in FACS buffer for flow cytometry analysis.

Cocultures of 4T1 cells and BMDCs. 2×10^4 4T1 cells were seeded to a 96-well plate, and incubated with different forms (free or liposome) and concentrations (high, medium or low) of DOX and R837 for 16 h. The supernatant was removed and cells were washed with HBSS. 4×10^4 BMDCs were added to each well and cocultured with 4T1 cells for another 16 h. BMDCs were harvested, washed, and stained with PE-Cy7-conjugated anti-CD11c, PE-conjugated anti-CD86, FITC-conjugated anti-MHCII, and Fixable Viability Dye eFluorTM 780 at 4°C for 30 min. After washing, cells were resuspended with 0.4% PFA and analyzed on a flow cytometer.

Tumor study. Balb/c mice (6-8 weeks) were subcutaneously inoculated with 4T1 tumor cells $(1x10^6 \text{ cells in } 50 \text{ μL HBSS})$ on day 0. On day 10 when the tumors grow to a size of ~100 mm³, mice were randomly divided into 4 groups: Ac₄ManNAz + DBCO-liposome, PBS + DBCO-liposomes, a mixture of Dox and R837, or PBS. Ac₄ManNAz (20 μL, 430 μg) or PBS was intratumorally injected. After 48 h, 20 μL of DBCO-liposome loaded with Dox (1 mg/mL) and R837 (0.5 mg/mL) or a bolus mixture of DOX and R837 was intratumorally injected. Three days later, tumors were collected, disrupted, digested, and resuspended in FACS buffer. Cells were then stained with the antibody cocktail at 4°C for 30 min, fixed with 0.4% PFA, and analyzed on a flow cytometer.

Statistical analyses. Statistical analysis was performed using GraphPad Prism v6 and v8. Sample variance was tested using the F test. For samples with equal variance, the significance between the groups was analyzed by a two-tailed student's t test. For samples with unequal variance, a two-tailed Welch's t-test was performed. For multiple comparisons, a one-way analysis of variance (ANOVA) with post hoc Fisher's LSD test was used. The results were deemed significant at $0.01 < *P \le 0.05$, highly significant at $0.001 < *P \le 0.01$, and extremely significant at $**P \le 0.001$.

Acknowledgements. The authors would like to acknowledge the financial support from NSF DMR 21-43673 CAR, R01CA274738, and the start-up package from the Department of Materials Science and Engineering at the University of Illinois at Urbana-Champaign and the Cancer Center at Illinois. Research reported in this publication was supported by the Cancer Scholars for Translational and Applied Research (C*STAR) Program sponsored by the Cancer Center at Illinois and the Carle Cancer Center under Award Number CST EP012023.

Competing Interests. The authors declare no competing financial interests.

Data Availability. Raw data can be accessed upon request, and will be published upon the acceptance of the manuscript.

REFERENCES

- Mellman, I., Coukos, G. & Dranoff, G. Cancer immunotherapy comes of age. *Nature* **480**, 480-489 (2011)
- 2 Couzin-Frankel, J. Cancer Immunotherapy. *Science* **342**, 1432-1433 (2013)
- Riley, R. S., June, C. H., Langer, R. & Mitchell, M. J. Delivery technologies for cancer immunotherapy. *Nat. Rev. Drug Discov.* **18**, 175-196 (2019)
- 4 Lesterhuis, W. J., Haanen, J. B. & Punt, C. J. Cancer immunotherapy—revisited. *Nat. Rev. Drug Discov.* **10**, 591-600 (2011)
- 5 Fukumura, D., Kloepper, J., Amoozgar, Z., Duda, D. G. & Jain, R. K. Enhancing cancer immunotherapy using antiangiogenics: opportunities and challenges. *Nat. Rev. Clin. Oncol.* **15**, 325-340 (2018)
- Zitvogel, L., Apetoh, L., Ghiringhelli, F. & Kroemer, G. Immunological aspects of cancer chemotherapy. *Nat. Rev. Immunol.* **8**, 59-73 (2008)
- Wang, Q. et al. Immunogenic cell death in anticancer chemotherapy and its impact on clinical studies. Cancer Lett. 438, 17-23 (2018)
- 8 Wu, J. & Waxman, D. J. Immunogenic chemotherapy: dose and schedule dependence and combination with immunotherapy. *Cancer Lett.* **419**, 210-221 (2018)
- 9 Liu, J. *et al.* Co-delivery of IOX1 and doxorubicin for antibody-independent cancer chemo-immunotherapy. *Nat. Commun.* **12**, 1-17 (2021)
- Wang, H. *et al.* Biomaterial-based scaffold for in situ chemo-immunotherapy to treat poorly immunogenic tumors. *Nat. Commun.* **11**, 1-14 (2020)
- Dong, X., Yang, A., Bai, Y., Kong, D. & Lv, F. Dual fluorescence imaging-guided programmed delivery of doxorubicin and CpG nanoparticles to modulate tumor microenvironment for effective chemo-immunotherapy. *Biomaterials* **230**, 119659 (2020)
- Lake, R. A. & Robinson, B. W. Immunotherapy and chemotherapy—a practical partnership. *Nat. Rev. Cancer* **5**, 397-405 (2005)
- Nowak, A. K., Robinson, B. W. & Lake, R. A. Synergy between chemotherapy and immunotherapy in the treatment of established murine solid tumors. *Cancer Res.* **63**, 4490-4496 (2003)
- Emens, L. A. & Middleton, G. The interplay of immunotherapy and chemotherapy: harnessing potential synergies. *Cancer Immunol. Res.* **3**, 436-443 (2015)
- Mu, W., Chu, Q., Liu, Y. & Zhang, N. A review on nano-based drug delivery system for cancer chemoimmunotherapy. *Nanomicro Lett.* **12**, 1-24 (2020)
- Ringgaard, L. *et al.* Tumor repolarization by an advanced liposomal drug delivery system provides a potent new approach for chemo-immunotherapy. *Sci. Adv.* **6**, eaba5628 (2020)
- 17 Chattopadhyay, S. *et al.* Synthetic immunogenic cell death mediated by intracellular delivery of STING agonist nanoshells enhances anticancer chemo-immunotherapy. *Nano Lett.* **20**, 2246-2256 (2020)
- Yong, S. B. *et al.* Dual-Targeted Lipid Nanotherapeutic Boost for Chemo-Immunotherapy of Cancer. *Adv. Mater.* **34**, 2106350 (2022)
- Liu, R., Li, X., Xiao, W. & Lam, K. S. Tumor-targeting peptides from combinatorial libraries. *Adv. Drug Deliv. Rev.* **110**, 13-37 (2017)
- Farokhzad, O. C., Karp, J. M. & Langer, R. Nanoparticle–aptamer bioconjugates for cancer targeting. *Expert Opin. Drug Deliv.* **3**, 311-324 (2006)
- Wang, H. *et al.* Selective in vivo metabolic cell-labeling-mediated cancer targeting. *Nat. Chem. Biol.* **13**, 415-424 (2017)

- Karamanos, N. K. *et al.* Extracellular matrix-based cancer targeting. *Trends Mol. Med.* **27**, 1000-1013 (2021)
- Gialeli, C., Theocharis, A. D. & Karamanos, N. K. Roles of matrix metalloproteinases in cancer progression and their pharmacological targeting. *FEBS J.* **278**, 16-27 (2011)
- Cathcart, J., Pulkoski-Gross, A. & Cao, J. Targeting matrix metalloproteinases in cancer: Bringing new life to old ideas. *Genes Dis.* **2**, 26-34 (2015)
- Golombek, S. K. *et al.* Tumor targeting via EPR: Strategies to enhance patient responses. *Adv. Drug Deliv. Rev.* **130**, 17-38 (2018)
- Park, J. *et al.* Tumor targeting using anti-her2 immunoliposomes. *J. Control. Release* **74**, 95-113 (2001)
- 27 Mittelheisser, V. *et al.* Optimal Physicochemical Properties of Antibody–Nanoparticle Conjugates for Improved Tumor Targeting. *Adv. Mater.* 2110305 (2022)
- Medina-Echeverz, J. *et al.* Synergistic cancer immunotherapy combines MVA-CD40L induced innate and adaptive immunity with tumor targeting antibodies. *Nat. Commun.* **10**, 1-12 (2019)
- 29 Chen, Q. *et al.* Photothermal therapy with immune-adjuvant nanoparticles together with checkpoint blockade for effective cancer immunotherapy. *Nat. Commun.* 7, 1-13 (2016)
- Zhou, S. *et al.* Engineering ApoE3-incorporated biomimetic nanoparticle for efficient vaccine delivery to dendritic cells via macropinocytosis to enhance cancer immunotherapy. *Biomaterials* **235**, 119795 (2020)
- Zhang, H. *et al.* Site-specific MOF-based immunotherapeutic nanoplatforms via synergistic tumor cells-targeted treatment and dendritic cells-targeted immunomodulation. *Biomaterials* **245**, 119983 (2020)
- Prescher, J. A., Dube, D. H. & Bertozzi, C. R. Chemical remodelling of cell surfaces in living animals. *Nature* **430**, 873-877, doi:10.1038/nature02791 (2004)
- Laughlin, S. T. & Bertozzi, C. R. Metabolic labeling of glycans with azido sugars and subsequent glycan-profiling and visualization via Staudinger ligation. *Nat. Protoc.* **2**, 2930 (2007)
- 34 Bhatta, R. *et al.* Recyclable cell-surface chemical tags for repetitive cancer targeting. *J. Control. Release* **347**, 164-174 (2022).
- Wang, H. *et al.* Metabolic labeling and targeted modulation of dendritic cells. *Nat. Mater.* **19**, 1244-1252 (2020)
- Wang, H. & Mooney, D. J. Metabolic glycan labelling for cancer-targeted therapy. *Nat. Chem.* **12**, 1102-1114 (2020)
- Wang, H. *et al.* Targeted Ultrasound-Assisted Cancer-Selective Chemical Labeling and Subsequent Cancer Imaging using Click Chemistry. *Angew. Chem. Int. Ed.* **55**, 5452-5456 (2016)
- Wang, H. *et al.* In vivo cancer targeting via glycopolyester nanoparticle mediated metabolic cell labeling followed by click reaction. *Biomaterials* **218**, 119305 (2019)
- Chang, P. V. *et al.* Copper-free click chemistry in living animals. *Proc. Natl. Acad. Sci.* **107**, 1821-1826 (2010)
- 40 Xie, R. *et al.* In vivo metabolic labeling of sialoglycans in the mouse brain by using a liposome-assisted bioorthogonal reporter strategy. *Proc. Natl. Acad. Sci.* **113**, 5173-5178 (2016)
- Baskin, J. M. *et al.* Copper-free click chemistry for dynamic in vivo imaging. *Proc. Natl. Acad. Sci.* **104**, 16793-16797 (2007)

- 42 Koo, H. *et al.* Bioorthogonal copper-free click chemistry in vivo for tumor-targeted delivery of nanoparticles. *Angewandte Chemie* **124**, 12006-12010 (2012)
- Liu, Z. et al. Cell membrane–camouflaged liposomes for tumor cell–selective glycans engineering and imaging in vivo. Proceedings of the National Academy of Sciences 118, e2022769118 (2021)
- Obeid, M. *et al.* Calreticulin exposure is required for the immunogenicity of γ -irradiation and UVC light-induced apoptosis. *Cell Death Differ.* **14**, 1848-1850 (2007)
- Zitvogel, L. *et al.* Immunogenic Tumor Cell Death for Optimal Anticancer Therapy: The Calreticulin Exposure PathwayThe Calreticulin Exposure Pathway. *Clin. Cancer Res.* **16**, 3100-3104 (2010)
- Garg, A. D. *et al.* A novel pathway combining calreticulin exposure and ATP secretion in immunogenic cancer cell death. *EMBO J.* **31**, 1062-1079 (2012)
- Wang, H. *et al.* Biomaterial-based scaffold for in situ chemo-immunotherapy to treat poorly immunogenic tumors. *Nat. Commun.* **11**, 5696 (2020)
- Zhou, F. *et al.* Tumor microenvironment-activatable prodrug vesicles for nanoenabled cancer chemoimmunotherapy combining immunogenic cell death induction and CD47 blockade. *Adv. Mater.* **31**, 1805888 (2019)
- 49 Kroemer, G., Galluzzi, L., Kepp, O. & Zitvogel, L. Immunogenic cell death in cancer therapy. *Annu. Rev. Immunol.* **31**, 51-72 (2013)